4-1985

Construction and Testing of a New Atomic Physics Beam Line at the Western Michigan University Accelerator Laboratory

William Andrew Hollerman
Western Michigan University

CONSTRUCTION AND TESTING OF A NEW ATOMIC PHYSICS BEAM LINE AT THE WESTERN MICHIGAN UNIVERSITY ACCELERATOR LABORATORY

by

William Andrew Hollerman

A Thesis
Submitted to the
Faculty of The Graduate College
in partial fulfillment of the
requirements for the
Degree of Master of Arts
Department of Physics

Western Michigan University
Kalamazoo, Michigan
April 1985

CONSTRUCTION AND TESTING OF A NEW ATOMIC PHYSICS BEAM LINE AT THE WESTERN MICHIGAN UNIVERSITY ACCELERATOR LABORATORY

William Andrew Hollerman, M.A.

Western Michigan University, 1985

A new beam line containing a differentially-pumped gas cell and charge state analyzing magnet was constructed for the purpose of measuring a wide variety of atomic inner-shell processes, such as excitation, ionization, and charge transfer. The completed system will be able to measure these individual atomic processes using coincidence techniques. Initial testing of the beam line was performed using 40 MeV S^{+7}+Ar collisions to determine the effect of the collimating slit size on the measured x-ray cross sections. These measurements showed that the slit size affects the x-ray cross section by a maximum of $\sim$6% between 4 mm^2 and $\geq$100 mm^2. X-ray production was measured for 30-60 MeV S^{+13}+Ar collisions to determine the relationship between cross section and beam energy. The results show that the x-ray cross section increases with beam energy. However, the measured cross sections were found to be about four times smaller than expected based on data obtained in another experiment.

ACKNOWLEDGMENTS

I would like to thank the entire faculty and staff of the Physics Department at Western Michigan University for all their help and support during my stay in Kalamazoo. I would especially like to thank Dr. John A. Tanis for being so patient with me during this project. I would also like to thank Mr. Marc Soller, Mr. Leo Parpart, and Mr. Scott Boman for assisting me in the construction and alignment phases of this thesis. I would like to give special consideration to my first physics teacher, Dr. David D. Chesak, for the use of his computer system in the data analysis. I would especially like to thank Dr. Larry Oppliger and Dr. Gene Bernstein for their time during the editing of this thesis. Finally, I would like to thank Mr. Chuck Mielke for his tireless effort in the machine shop. He always gave this project his typical "$1.98" worth of work!

William Andrew Hollerman

INFORMATION TO USERS

This reproduction was made from a copy of a document sent to us for microfilming. While the most advanced technology has been used to photograph and reproduce this document, the quality of the reproduction is heavily dependent upon the quality of the material submitted.

The following explanation of techniques is provided to help clarify markings or notations which may appear on this reproduction.

1. The sign or "target" for pages apparently lacking from the document photographed is "Missing Page(s)". If it was possible to obtain the missing page(s) or section, they are spliced into the film along with adjacent pages. This may have necessitated cutting through an image and duplicating adjacent pages to assure complete continuity.

2. When an image on the film is obliterated with a round black mark, it is an indication of either blurred copy because of movement during exposure, duplicate copy, or copyrighted materials that should not have been filmed. For blurred pages, a good image of the page can be found in the adjacent frame. If copyrighted materials were deleted, a target note will appear listing the pages in the adjacent frame.

3. When a map, drawing or chart, etc., is part of the material being photographed, a definite method of "sectioning" the material has been followed. It is customary to begin filming at the upper left hand corner of a large sheet and to continue from left to right in equal sections with small overlaps. If necessary, sectioning is continued again—beginning below the first row and continuing on until complete.

4. For illustrations that cannot be satisfactorily reproduced by xerographic means, photographic prints can be purchased at additional cost and inserted into your xerographic copy. These prints are available upon request from the Dissertations Customer Services Department.

5. Some pages in any document may have indistinct print. In all cases the best available copy has been filmed.

University Microfilms International
300 N. Zeeb Road
Ann Arbor, MI 48106

Hollerman, William Andrew

CONSTRUCTION AND TESTING OF A NEW ATOMIC PHYSICS BEAM LINE AT THE WESTERN MICHIGAN UNIVERSITY ACCELERATOR LABORATORY

Western Michigan University M.A. 1985

TABLE OF CONTENTS

LIST OF TABLES

LIST OF FIGURES

CHAPTER I

INTRODUCTION

Several basic inner-shell processes occur in heavy ion-atom collisions, such as excitation, ionization, and charge transfer. Excitation is the general term for any process where electrons are raised to higher energy levels. This process can be experimentally observed by detecting the photon from the resulting de-excitation. Ionization is simply the extension of excitation; here the electron is given sufficient energy to remove it from the atom and place it in the continuum. As with excitation, ionization can be observed by detecting the energy of the emitted photon when the vacancy is filled by another electron. The third type of inner-shell process is called charge transfer. Charge transfer occurs when the projectile ion exchanges electrons with the target atom. These charge-changing events can be observed by using a magnetic or electric field to separate the various charge state components of the beam emerging from the target. A particle detector is positioned so the field will bend the selected charge-state into the detector. Electronic coincidences between the charge-changed ions and photons emitted in the target are used to separate the individual atomic processes mentioned above.

In the last several years, a particular type of charge-changing event has been a topic of great interest.[1,2] When electron capture is accompanied by a simultaneous K-shell excitation in the projectile

ion, the process is called resonant transfer and excitation (RTE). The desire for an apparatus that could measure RTE prompted the design and construction of the new gas cell target and beam line. This apparatus can also be used to investigate any of the three basic atomic processes listed above as well as total electron capture and loss probabilities.

This thesis will describe the design and construction of the gas cell target and beam line system at the Western Michigan University Accelerator Laboratory. It includes the results of the initial testing of the apparatus using S+Ar collisions. Data are presented which examine the effect of beam collimating slit size on the x-ray cross sections. Other data compare the measured x-ray cross section versus beam energy to previous experimental results.[2]

CHAPTER II

DESCRIPTION OF THE BEAM LINE AND GAS CELL

The work described below was performed at Western Michigan University using the 6 MV model EN tandem Van de Graaff accelerator. Figure 1 shows a schematic diagram of the entire beam line with the gas cell in place. Following the selection of the desired charge state from the accelerator, the beam was collimated with two sets of adjustable slits placed two meters apart. Each unit has four individual micrometer paddles which define the beam in both the horizontal and vertical plane of collimation. The individual micrometer assembly can be adjusted independently to achieve almost any desired slit area. Both sets of slits are electrically insulated from the surrounding beam pipe so that ion current measurements can be taken.

After collimation with the adjustable slits, the beam strikes a gas target contained inside a differentially-pumped gas cell. The purpose of the differentially-pumped cell is to maintain a relatively high target gas pressure and to keep this gas from significantly raising the surrounding beam line pressure. This is accomplished in two stages; first, gas which escapes from the target cell through its entrance and exit apertures enters a region pumped by a 4" diffusion pump (see Figure 1). The gas in this region is restricted from entering the beam line by two apertures as shown in Figure 1. The area of the opening leading to the 4" diffusion pump is much larger

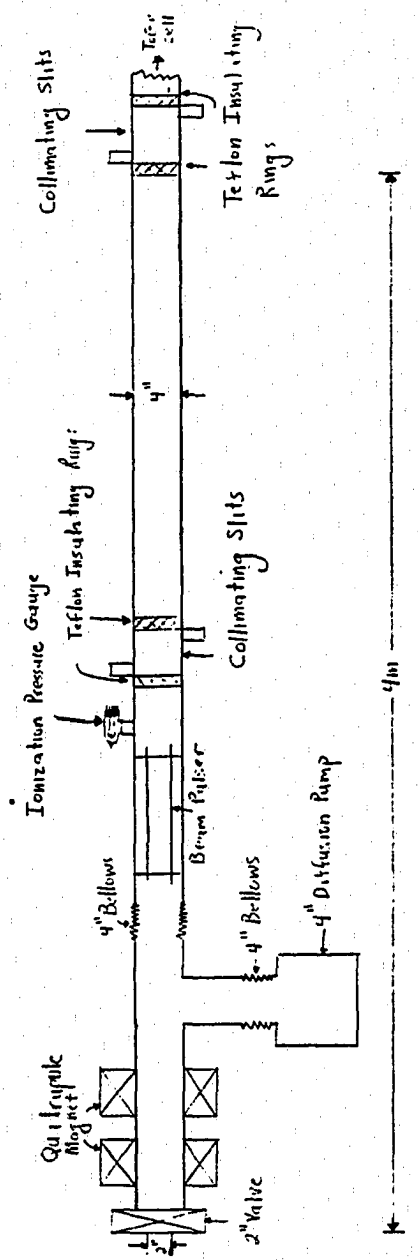

Figure 1. New Atomic Physics Beam Line, WMU (Page 1 of 2)

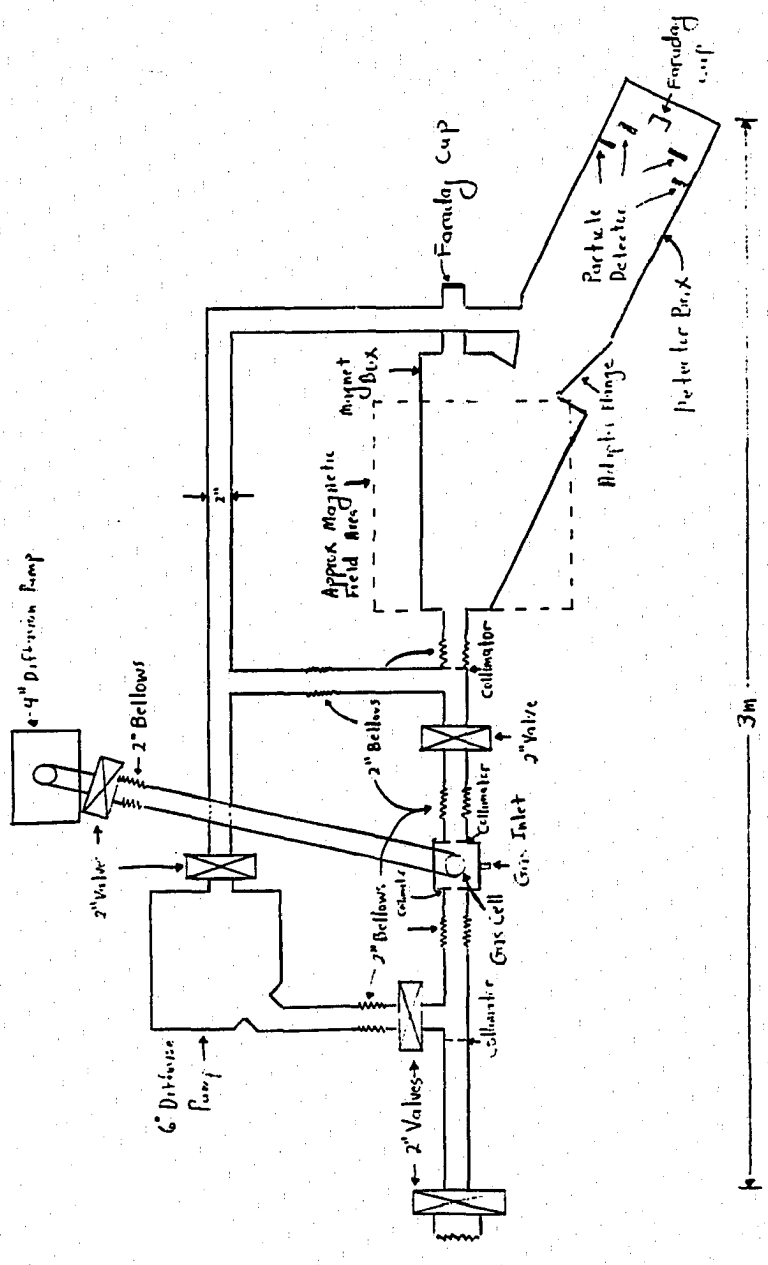

Figure 2. New Atomic Physics Beam Line, WMU (Page 2 of 2)

than the corresponding area of the two apertures. Hence, target gas is more likely to escape to the 4" diffusion pump than through the aperture openings. The small amount of target gas that does escape through the apertures is differentially-pumped a second time using a 6" diffusion pump and collimating apertures as shown in Figure 1. Target gas pressure is measured with a capacitance manometer. Pressures of 0-50 microns of argon gas were present for the cross section measurements which will be discussed below. The resulting x-rays which are produced in the gas cell are detected with a Si(Li) detector mounted at 90° to the incident beam direction.

At the present time, this is the extent of the completed construction of the beam line, although the other components of the apparatus (see Figure 1), such as the magnet box, ion detector system, and vacuum system, are ready to be installed. Future plans include the installation of a 17.5 kilogauss spectroscopy magnet downstream of the gas cell to separate the emerging beam into charge state components. An array of four surface barrier detectors placed behind the magnet will measure the ion flux which is present in four particular charge states, namely Q-2, Q-1, Q+1, and Q+2 with Q being the incident charge of the ion beam. The detector assembly, in conjunction with the magnet, was designed to charge analyze ions as heavy as bromine with kinetic energies as high as 80MeV. The addition of the particle detection system described above makes it possible to directly measure charge-changing atomic interactions.

Alignment

The alignment of the beam line was accomplished in two distinct

parts: alignment of the quadrupole magnet and alignment of the collimating slits. Initially, the alignment of the quadrupole was performed by focusing an optical telescope (which was aligned on the output port of the switching magnet) on the geometric center of the magnet's pole pieces. Final adjustments to the alignment were made using a 3 MeV proton beam incident on a quartz crystal to allow direct optical viewing of the ion beam. A charged ion beam should exit a properly aligned quadrupole without being steered by the magnet. Any deviation in position of the ion beam after passing through the quadrupole indicates a misalignment of the device. The quadrupole was then moved until the 3 MeV proton beam was not steered by the magnetic field. The effect of the quadrupole on the beam intensity was checked using a Faraday cup in place of the quartz crystal. The quadrupole coil current (which varies the magnetic field) was adjusted until the ion beam current reached a maximum value. Table 1 shows the resulting data: the beam intensity using both the 3 MeV proton and 20 MeV fluorine beams was increased between fifty to seventy-five percent when the quadrupole was operational. The procedure for the alignment of the collimating slits can be found in Appendix A. After the alignment procedure was completed, the optical telescope was lined up with the centers of the two slits. Future beam alignment is now possible using the telescope.

Electronics and Computer System

A diagram of the electronic components used in the x-ray cross section measurements is shown in Figure 2. The signal output from

Table 1

Target Quadrupole Alignment Data

Trial	Beam	Beam Energy (MeV)	Analyzing Cup Current (nA)	Target Quad. Beam Current (A) L	R	Target Beam Current (nA)	Increase of Beam Current (%)
1	H^{+1}	3	220	0		120	50
				6.0	6.5	180	
2	H^{+1}	3	220	0		120	75
				6.0	6.5	210	
3	F^{+4}	20	350	0		13	69
				9.5	12.0	22	
4	F^{+4}	20	175	0		15	67
				9.5	7.5	25	

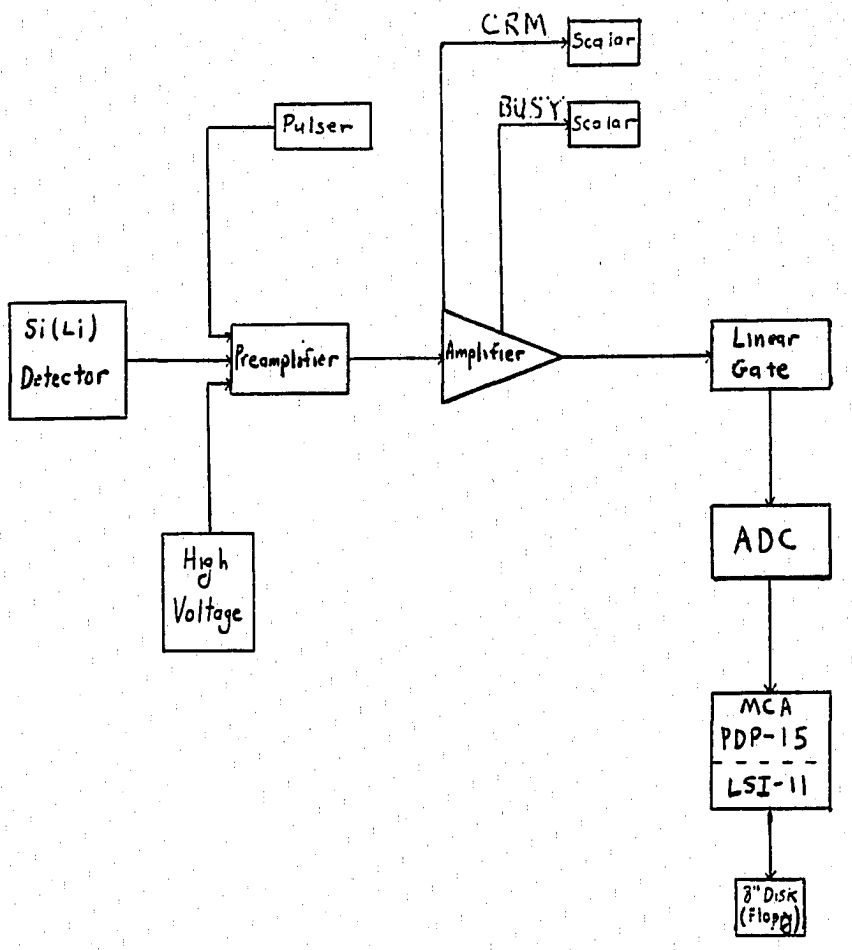

Figure 2. Diagram of Electronic Apparatus

the Si(Li) detector first passes through a preamplifier which increases the amplitude of the generated pulses. The high voltage for the Si(Li) detector is connected to an auxiliary input of the preamplifier. A signal pulser is attached to a separate preamplifier input which allows for the testing of the entire electronics system without a source being present. The output of the preamplifier is connected to an Ortec 739 amplifier which further increases the amplitude of the signals; the amplifier also shapes the pulse so it is acceptable for input to the linear gate. Two scalars, individually connected to the CRM and BUSY outputs of the amplifier, measure the dead time of the electronics. An Ortec 442 linear gate sets a low energy threshold to eliminate the noise and low amplitude signals from the x-ray pulses. The output signal from the linear gate is sent into an ADC which provides a digital output for input to a multichannel analyzer; this analyzer is interfaced to a PDP-15 computer. The resulting x-ray spectra are stored on an eight-inch floppy disk which is controlled by a program in an LSI-11 microcomputer.

CHAPTER III

DATA ANALYSIS AND RESULTS

Initial testing of the beam line was performed using a 40 MeV S^{+7}+Ar reaction to check the alignment of the system and look for the effects of beam collimation and slit scattering on the measured x-ray production cross sections. Additional measurements were made for 30, 40, 48, and 60 MeV S^{+13}+Ar collisions to compare the x-ray cross sections with previous results. A typical spectrum consists of three distinct peaks: the sulfur K_α, argon K_α, and argon K_β x rays at about 2.30, 2.96, and 3.19 keV respectively. Figure 3 shows a typical spectrum. The number of x rays in these individual peaks was obtained by summing the counts under each peak. The x-ray production cross section can be thought of as the probability of an x ray being produced in the interaction of a projectile ion with the target atom. The total x-ray production cross section is a function of several different parameters which are given below.

$$N_{x\text{-rays}} = I_0 \sigma_x N \ell P \frac{\Delta\Omega}{4\pi} \varepsilon \qquad (1)$$

Where: $N_{x\text{-rays}}$ = Number of X-rays in Peak

I_0 = Incident Ion Flux

$N = 3.30 \times 10^{13} \frac{\text{atoms}}{\mu \cdot \text{cm}^3}$

ℓ = Target Length

P = Gas Cell Pressure

$\Delta\Omega$ = Detector Solid Angle

ε = X-Ray Detection Efficiency

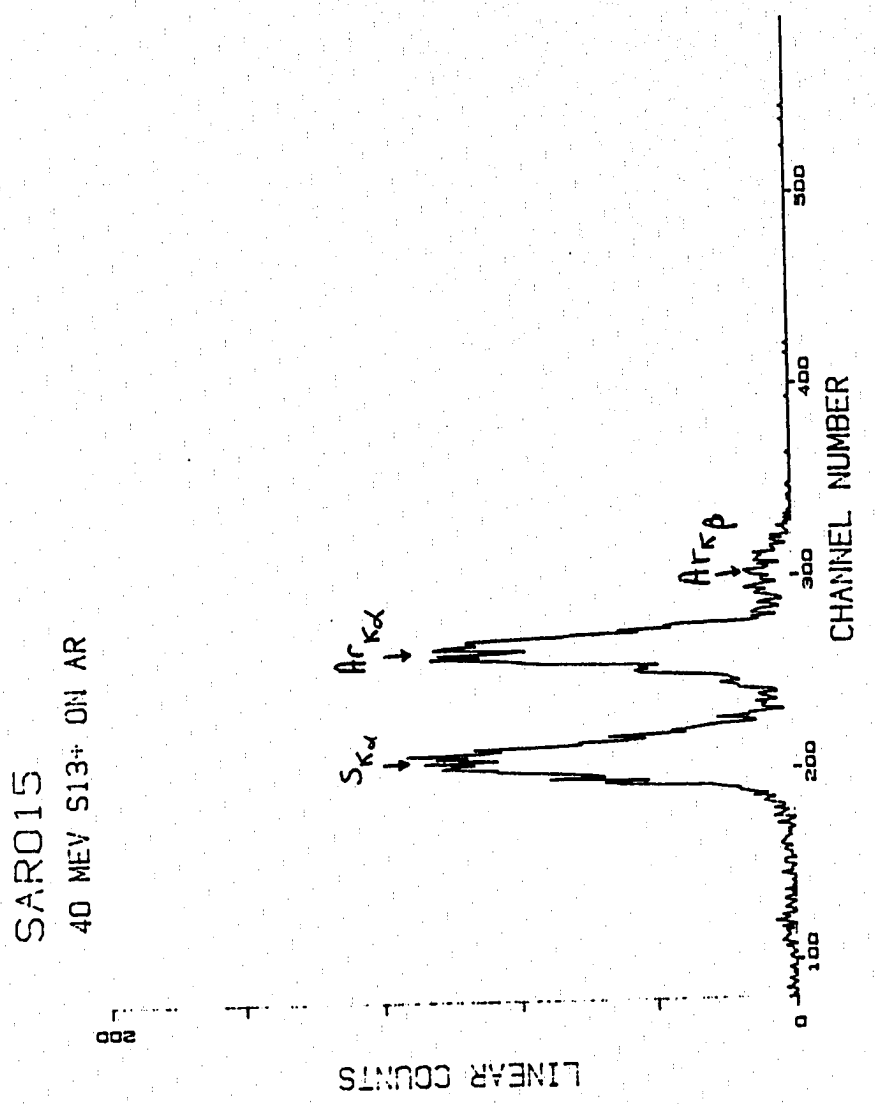

Figure 3. Sample Spectrum from MCA

Then:

$$F \equiv \frac{N_{x\text{-rays}}}{I_0} = \sigma_x N P \ell \frac{\Delta\Omega}{4\pi} \varepsilon \qquad (2)$$

Where: F = Fraction of X-Rays to Incident Ions

All of the x-ray cross section measurements presented in this paper assume that the incident sulfur ions have only one interaction with the argon target gas in the gas cell. This assumption is valid for "low" gas cell pressures. In this case the fraction F is a linear function of the gas cell pressure.

$$\Delta F = \sigma_x N \ell \frac{\Delta\Omega}{4\pi} \varepsilon \Delta P \qquad (3)$$

Where: ΔF = Change in the X-Ray Fraction F

ΔP = Change in the Gas Cell Pressure P

Equation (3) can be solved for σ_x to give the expression for the x-ray production cross section.

$$\sigma_x = \frac{(\frac{\Delta F}{\Delta P})}{N \ell \frac{\Delta\Omega}{4\pi} \varepsilon} \qquad (4)$$

Where: $(\frac{\Delta F}{\Delta P})$= Slope of Graph when F is Plotted Versus P

Appendix B gives a detailed explanation of how σ_x is calculated for the sulfur K_α, argon K_α, and argon K_β x rays. The quantity ε in equation (4) represents the x-ray detection efficiency. The thin (0.001 inch) beryllium window on the Si(Li) detector attenuates some of the x rays which are produced in the gas cell so that the number of detected x rays is less than the number of x rays produced in the target. Appendix C gives a complete derivation of the attenuation coefficients for the sulfur K_α, argon K_α, and argon K_β x rays.

Appendix D gives a sample calculation of the x-ray production cross section using all of the above mentioned components.

CHAPTER IV

DISCUSSION

Effect of Beam Collimation

The effect of beam collimation on the x-ray cross sections was studied for 40 MeV S^{+7}+Ar collisions. The results can be found in Table 2 below. The x-ray production cross section was measured with both a $\geq 100\ mm^2$ and a $4\ mm^2$ slit opening. Notice that the difference in collimating slit area affects the x-ray cross section by approximately 6%. This difference is less than the size of the error bars on the x-ray cross section data between a slit area of $\geq 100\ mm^2$ and $4\ mm^2$. These data also show that the cross section for the $4\ mm^2$ slit opening is consistently larger than the similar measurements taken at $\geq 100\ mm^2$. This systematic increase in x-ray cross section might be caused by slit scattering of the incident sulfur ions.

Table 2

40 MeV S^{+7}+Ar Slit Comparison Data

X-Ray	σ_{4mm^2} (x $10^{-20} cm^2$)	σ_{OPEN} (x $10^{-20} cm^2$)	$\sigma_{OPEN}/\sigma_{4mm^2}$
Sulfur K_α	1.38 ± 0.10	1.30 ± 0.04	0.94 ± 0.08
Argon K_α	0.906 ± 0.096	0.863 ± 0.043	0.95 ± 0.11
Argon K_β	0.114 ± 0.012	0.107 ± 0.005	0.94 ± 0.11

The results in Table 2 above can be compared with data taken by Winters, et al. which measured the S_K and Ar_K x-ray production cross sections to be 1.30 x 10^{-20} cm^2 (±50%) and 0.50 x 10^{-20} cm^2 respectively, at 16.5 MeV for a S^{+7}+Ar collision.[3] The values of the cross sections in Table 2 are of the same order of magnitude as the Winters, et al. data.

X-Ray Production for 30-60 MeV S^{+13}+Ar Collisions

Results from the x-ray production cross section measurements for 30-60 MeV S^{+13}+Ar collisions can be found in Table 3 below. These data show that the production cross section is steadily increasing over the energy range of 30-60 MeV for the sulfur K_α, argon K_α, and argon Kβ x rays. This result is consistent with other measurements of the x-ray production cross section for S^{+13}+Ar collisions.[1,2,4]

Table 3

30-60 MeV S^{+13}+Ar Energy Comparison Data

Beam Energy (MeV)	$\sigma_{S_{K_\alpha}}$ (x 10^{-20} cm^2)	$\sigma_{Ar_{K_\alpha}}$ (x 10^{-20} cm^2)	$\sigma_{Ar_{K_\beta}}$ (x 10^{-21} cm^2)
30	2.85 ± 0.43	1.77 ± 0.44	2.13 ± 0.30
40	3.11 ± 0.43	2.44 ± 0.35	3.75 ± 0.23
48	3.51 ± 0.38	2.89 ± 0.33	3.93 ± 0.43
60	4.41 ± 0.36	3.24 ± 0.38	4.18 ± 0.55

A plot of the results in Table 3 can be found in Figure 4. This

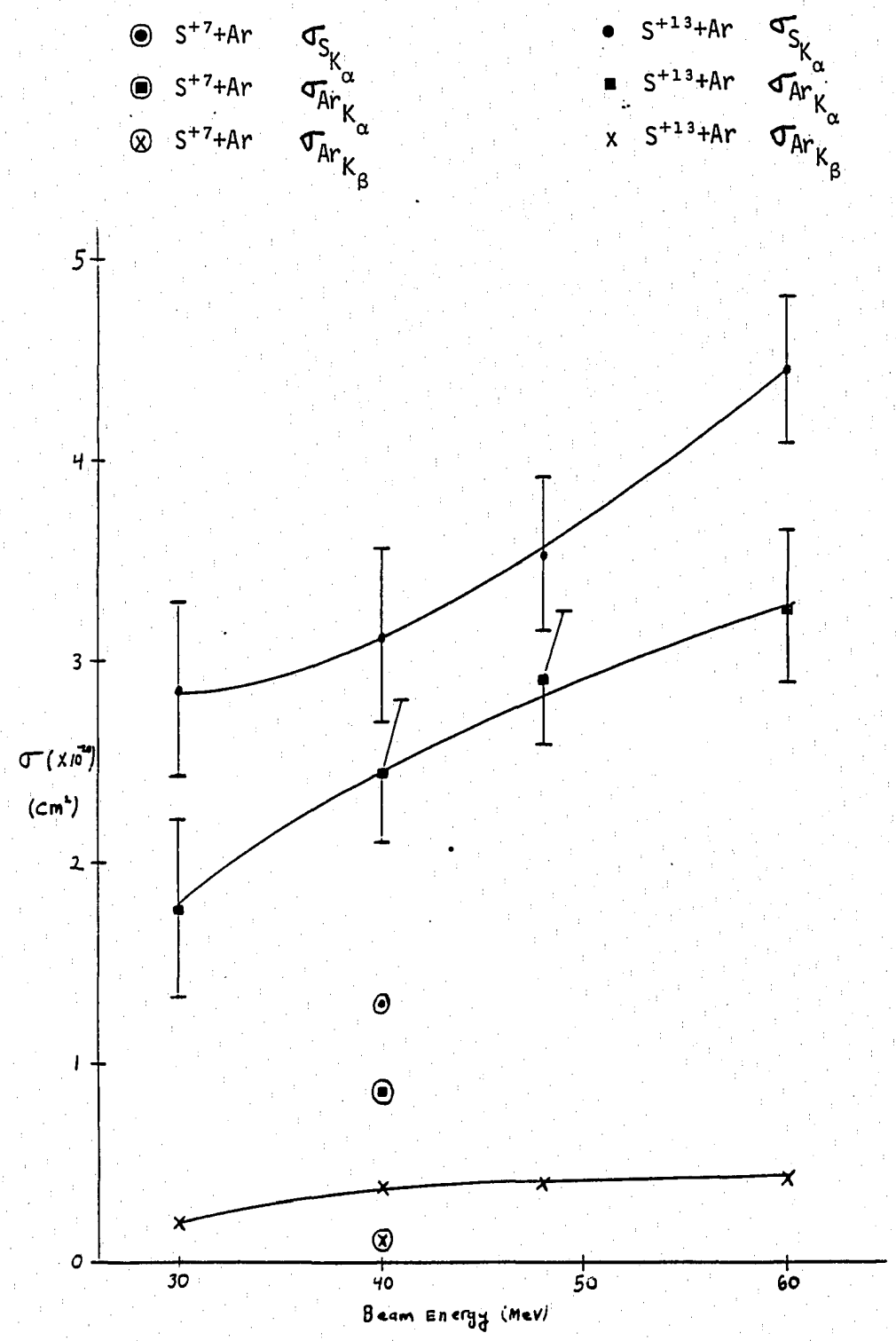

Figure 4. Plot of S^{+13}+Ar Data

plot also includes the S^{+7}+Ar data at 40 MeV for comparison. Extrapolation of data taken in a similar experiment by Tanis, et al. indicates that both the sulfur K_α and argon K_α x-ray production cross section increases smoothly with increasing beam energy.[2] Comparison with the Tanis, et al. data shows that the sulfur K_α and argon K_α x-ray cross sections shown in Table 3 are between three to five times smaller than previously measured values for these x-ray cross sections.[2] A plot showing the relationship of the Tanis, et al. data to the measurements listed in Table 3 is given in Figure 5. At the present time there is no explanation for these large differences in the x-ray production cross section. Further measurements of the x-ray cross section should be taken between 30 and 160 MeV to resolve this question.

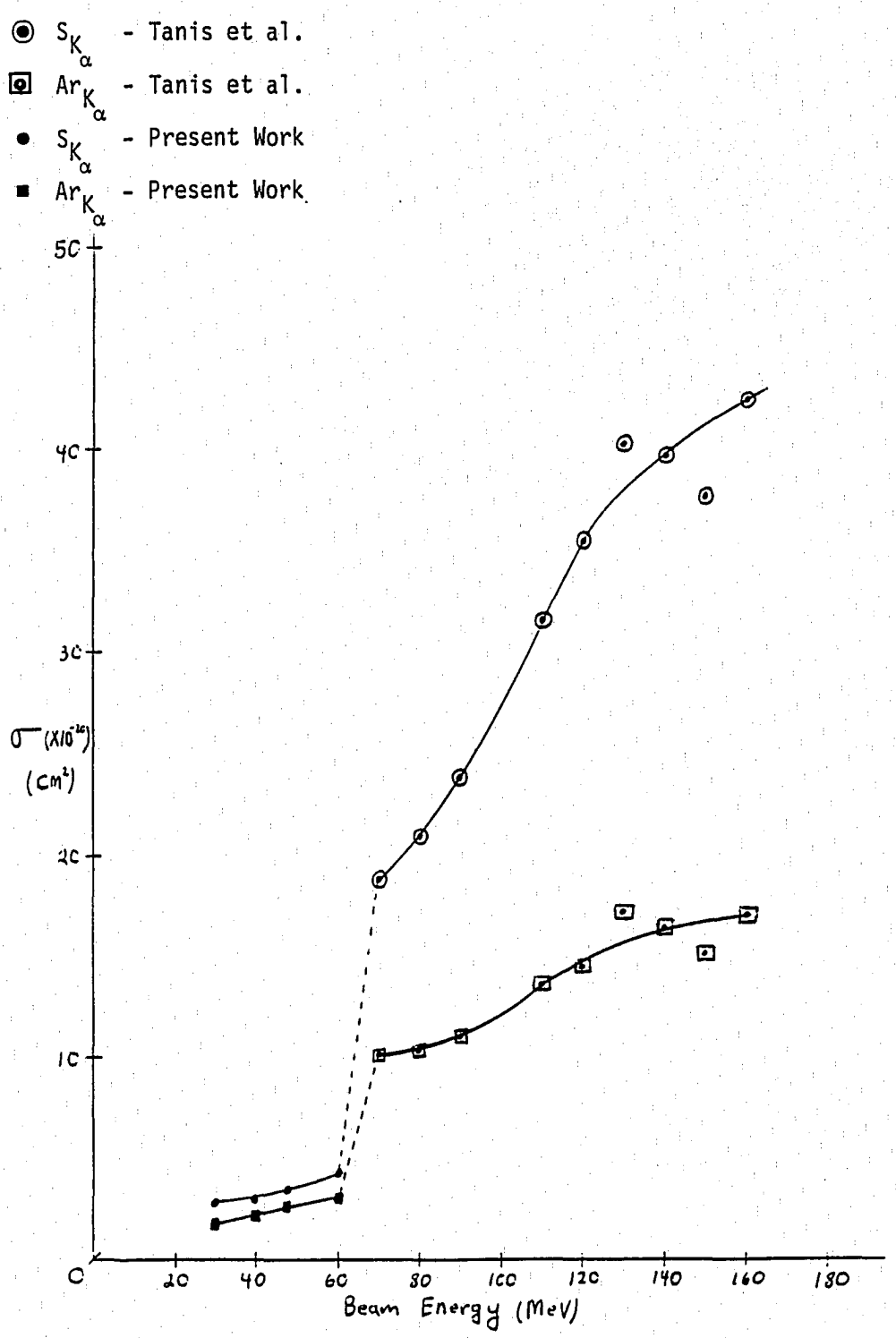

Figure 5. Plot Comparing Tanis, et al. Data[2] and Present Data

CHAPTER V

CONCLUSION

A new beam line with a differentially-pumped gas cell was constructed at the Western Michigan University Accelerator Laboratory. Magnetic analysis will be used to separate the charge state components of the beam which emerges from the gas cell. This beam line will be used to measure the individual atomic processes of excitation, ionization, and charge transfer in ion-atom collisions. Data taken at 40 MeV for S^{+7}+Ar collisions showed that collimating slit size had only a small ($\sim$6%) effect on the x-ray cross section measurements. Data taken for S^{+13}+Ar collisions showed that the sulfur K_{α}, argon K_{α}, and argon K_{β} x ray production cross sections each increased with beam energy between 30 and 60 MeV. The measured cross sections were found to be approximately three to five times smaller than expected from previous results. Further measurements are necessary to resolve this large discrepancy in the data.

REFERENCES

1. Tanis, J.A., Shafroth, S.M., Willis, J.E., Clark, M., Swenson, J., Strait, E.N., and Mowat, J.R., Phys. Rev. Lett. 47, 828 (1981).

2. Tanis, J.A., Bernstein, E.M., Graham, W.G., Clark, M., Shafroth, S.M., Johnson, B.M., Jones, K.W., and Meron, M., Phys. Rev. Lett. 49, 1325 (1982).

3. Winters, L., Brown, M.D., Ellsworth, L.D., Chiao, T., Pettus, E.W., and Macdonald, J.R., Phys. Rev. A 11, 174 (1975).

4. Macdonald, J.R., Brown, M.D., Czuchlewski, S.J., Winters, L.M., Laubert, R., Sellin, I.A., and Mowat, J.R., Phys. Rev. A 14, 1997 (1976).

5. Acosta, V., Cowan, C.L., and Graham, B.J., Essentials of Modern Physics. New York: Harper and Row, Publishers, 1973.

6. Storm, E., and Israel, H.I., Nuclear Data Tables, A 7, 565 (1970).

7. Weast, R.C., and Astle, M.J., eds., CRC Handbook of Chemistry and Physics, 59th Edition. Palm Beach: CRC Press, Inc., 1979.

APPENDIX A

Gas Cell Collimating Slit Alignment Procedure

The procedure below lists the steps which were used to align the collimating slits with the actual beam position. Once this line between the collimating slits has been established, further construction can use the slits for alignment purposes.

1. Accelerate the desired beam with the target room quadrupole turned off. With the downstream slits closed, maximize the beam on the slits using the low energy steerers, high energy quadrupoles, source controls, and other accelerator controls.

2. After the beam is maximized on the downstream slits, open them up and observe the beam on a quartz plate. A true beam axis is now defined. A pointer fixed in space is placed in the center of the beam spot on the quartz. This locates the beam in space.

3. Set all four of the upstream micrometers to a one millimeter opening.

4. Adjust the beam line position until the hole created by the upstream slits is centered on the pointer.

5. Open the upstream slits wide open and repeat steps three and four for the downstream slit assembly.

6. Open the downstream slits and repeat the procedure outlined in

steps three, four, five, and six as many times as necessary until both sets of slits are centered on the pointer.

APPENDIX B

Calculations of X-Ray Cross Sections

Equation 4 on page 13 of the text gives the form of the cross section expression which is used in these measurements.

$$\sigma_x = \frac{(\frac{\Delta F}{\Delta P})}{N\ell(\frac{\Delta\omega}{4\pi})\varepsilon} \qquad (1B)$$

The quantity $(\frac{\Delta F}{\Delta P})$ is the slope of the x-ray fraction versus pressure graph (see Appendix D). The value of N is given as the number of atoms of target gas per unit volume per unit pressure:

$$N = 3.3 \times 10^{13} \text{ atoms}/\mu\cdot\text{cm}^3$$

The parameter ℓ is the length of the target gas cell:

$$\ell = 2.778 \text{ cm}$$

The quantity $(\frac{\Delta\omega}{4\pi})$ is the ratio of the detector solid angle to the solid angle of all space (4π steradians). Since our detector subtends an angle smaller than all space, a correction factor must be used in the cross section calculation. The detector is only detecting a fraction of the total emitted x rays since the detector subtends a small portion of the total solid angle. It has been assumed that the source of the x rays is isotropic. The value of $\Delta\omega$ determined by numerical integration for the present geometry is:

$$\Delta\omega = 0.101 \text{ steradians}$$

The parameter ε gives the detection efficiencies for each of the three x-rays:

$$\varepsilon_{S_{K_\alpha}} = 0.812$$
$$\varepsilon_{Ar_{K_\alpha}} = 0.910$$
$$\varepsilon_{Ar_{K_\beta}} = 0.928$$

These quantities are derived in Appendix C. Since all the parameters except the quantity $(\frac{\Delta F}{\Delta P})$ are known, let us combine all the other constants together:

$$\sigma_x = \frac{1}{N\ell(\frac{\Delta}{4\pi})} \left[\frac{(\frac{\Delta F}{\Delta P})}{\varepsilon} \right]$$

$$\sigma_x = 1.36 \times 10^{-12} \left[\frac{(\frac{\Delta F}{\Delta P})}{\varepsilon} \right] \quad (cm^2) \qquad (2B)$$

Sulfur K_α x-ray: $\varepsilon_{S_{K_\alpha}} = 0.812$

Equation (2B) $\rightarrow \sigma_{S_{K_\alpha}} = (1.36 \times 10^{-12}) (\frac{1}{0.812}) (\frac{\Delta F}{\Delta P})_{S_{K_\alpha}} \quad (cm^2)$

$$\therefore \boxed{\sigma_{S_{K_\alpha}} = 1.67 \times 10^{-12} (\frac{\Delta F}{\Delta P})_{S_{K_\alpha}} \quad (cm^2)} \qquad (3B)$$

Argon K_α x-ray: $\varepsilon_{Ar_{K_\alpha}} = 0.910$

Equation (2B) $\rightarrow \sigma_{Ar_{K_\alpha}} = 1.36 \times 10^{-12} (\frac{1}{0.910}) (\frac{\Delta F}{\Delta P})_{Ar_{K_\alpha}} \quad (cm^2)$

$$\therefore \boxed{\sigma_{Ar_{K_\alpha}} = 1.49 \times 10^{-12} \left(\frac{\Delta F}{\Delta P}\right)_{Ar_{K_\alpha}} \quad (cm^2)} \qquad (4B)$$

Argon K_β x-ray: $\varepsilon_{Ar_{K_\beta}} = 0.928$

Equation (2B) $\rightarrow \sigma_{Ar_{K_\beta}} = 1.36 \times 10^{-12} \left(\frac{1}{0.928}\right) \left(\frac{\Delta F}{\Delta P}\right)_{Ar_{K_\beta}} \quad (cm^2)$

$$\therefore \boxed{\sigma_{Ar_{K_\beta}} = 1.46 \times 10^{-12} \left(\frac{\Delta F}{\Delta P}\right)_{Ar_{K_\beta}} \quad (cm^2)} \qquad (5B)$$

Equations (3B), (4B), and (5B) can be used to calculate the corresponding x-ray cross section when $\left(\frac{\Delta F}{\Delta P}\right)$ is calculated from the data.

Units Check

The units on each of the cross section equations is cm^2. The units on the quantity $\frac{\Delta F}{\Delta P}$ is μ^{-1} (inverse pressure in microns). The units on the constant coefficient given in equation (2B) is $cm^2 \cdot \mu$.

So: $(cm^2) = \frac{1}{\frac{1}{cm^3 \cdot \mu}} \cdot \frac{1}{(\frac{sr}{sr})cm} \cdot \mu^{-1}$

$(cm^2) = cm^2 \cdot \mu \cdot \mu^{-1} = cm^2$ □

APPENDIX C

Beryllium Attenuation Coefficients and Detector Efficiency

The intensity of x rays emitted from the gas cell is reduced by absorption through a thin beryllium window which covers the Si(Li) detector. The absorption coefficient (μ) is used as a measure of the attenuation by the beryllium.[6]

$$dN = -\mu N dx \tag{1C}$$

where: μ = Absorption Coefficient

N = Number of Transmitted X Rays

dx = Incremental Thickness of Absorber

dN = Change in Number of Transmitted X Rays

Then:

$$\int \frac{dN}{N} = -\int \mu dx$$

$$\ln N - \ln N_0 = -\mu x \qquad N_0 = \text{Initial Number of X Rays (Constant of Integration)}$$

$$\ln\left(\frac{N}{N_0}\right) = -\mu x$$

$$\frac{N}{N_0} = e^{-\mu x}$$

Define: $\varepsilon \equiv \frac{N}{N_0}$ Efficiency of Detection

$$\therefore \boxed{\varepsilon = \frac{N}{N_0} = e^{-\mu x}} \tag{2C}$$

The absorption coefficient μ is a function of both the x-ray energy and the absorbing material.

Mass Absorption Coefficients for ^{4}Be Window[6]

X-Ray Energy (keV)	$\mu(\frac{cm^2}{g})$	lnE	lnμ
1.0	595.5	0	6.389
1.5	177.8	0.405	5.181
2.0	72.84	0.693	4.288
3.0	19.78	1.099	2.985
4.0	7.75	1.386	2.048
5.0	3.73	1.609	1.316
6.0	2.07	1.792	0.728

Least Squares Fit:

$$\ln\mu = -3.18 \ln E + 6.44$$ (see Figure 6 on page 31)

Calculation of μ for each type of x ray:

S_{K_α} x ray $\quad E_{S_{K_\alpha}} = 2.31$ keV

Ar_{K_α} x ray $\quad E_{Ar_{K_\alpha}} = 2.96$ keV

Ar_{K_β} x ray $\quad E_{Ar_{K_\alpha}} = 3.19$ keV

$$S_{K_\alpha} \rightarrow \ln\mu_{S_{K_\alpha}} = -3.18 \ln(2.31) + 6.44 \ (\frac{cm^2}{g})$$

$$\ln\mu_{S_{K_\alpha}} = 3.79$$

$$\boxed{\mu_{S_{K_\alpha}} = 44.3 \frac{cm^2}{g}}$$

$$Ar_{K_\alpha} \rightarrow \ln\mu_{Ar_{K_\alpha}} = -3.18 \ln(2.96) + 6.44 \left(\frac{cm^2}{g}\right)$$

$$\ln\mu_{Ar_{K_\alpha}} = 3.00$$

$$\boxed{\mu_{Ar_{K_\alpha}} = 20.1 \frac{cm^2}{g}}$$

$$Ar_{K_\beta} \rightarrow \ln\mu_{Ar_{K_\beta}} = -3.18 \ln(3.19) + 6.44 \left(\frac{cm^2}{g}\right)$$

$$\ln\mu_{Ar_{K_\beta}} = 2.76$$

$$\boxed{\mu_{Ar_{K_\beta}} = 15.8 \frac{cm^2}{g}}$$

The units on μ must be inverse length for use in equation (2C). This conversion can be made by multiplying each of the above values by the density of beryllium.[7]

$$\rho_{Be} = 1.85 \text{ g/cm}^3 \qquad x = 0.001 \text{ in} = 2.54 \times 10^{-3} \text{ cm}$$

Detection Efficiency $\varepsilon = \frac{N}{N_0} = e^{-\mu x}$ [equation (2C)]

$$S_{K_\alpha} \rightarrow \varepsilon_{S_{K_\alpha}} = \exp\left[-\left(44.3 \frac{cm^2}{g}\right)\left(1.85 \frac{g}{cm^3}\right)\left(2.54 \times 10^{-3}\ cm\right)\right]$$

$$\boxed{\varepsilon_{S_{K_\alpha}} = 0.812}$$

$$Ar_{K_\alpha} \rightarrow \varepsilon_{Ar_{K_\alpha}} = \exp\left[-\left(20.1 \frac{cm^2}{g}\right)\left(1.85 \frac{g}{cm^3}\right)\left(2.54 \times 10^{-3}\ cm\right)\right]$$

$$\boxed{\varepsilon_{Ar_{K_\alpha}} = 0.910}$$

$$Ar_{K_\beta} \rightarrow \varepsilon_{Ar_{K_\beta}} = \exp\left[-\left(15.8 \frac{cm^2}{g}\right)\left(1.85 \frac{g}{cm^3}\right)\left(1.54 \times 10^{-3}\ cm\right)\right]$$

$$\boxed{\varepsilon_{Ar_{K_\beta}} = 0.928}$$

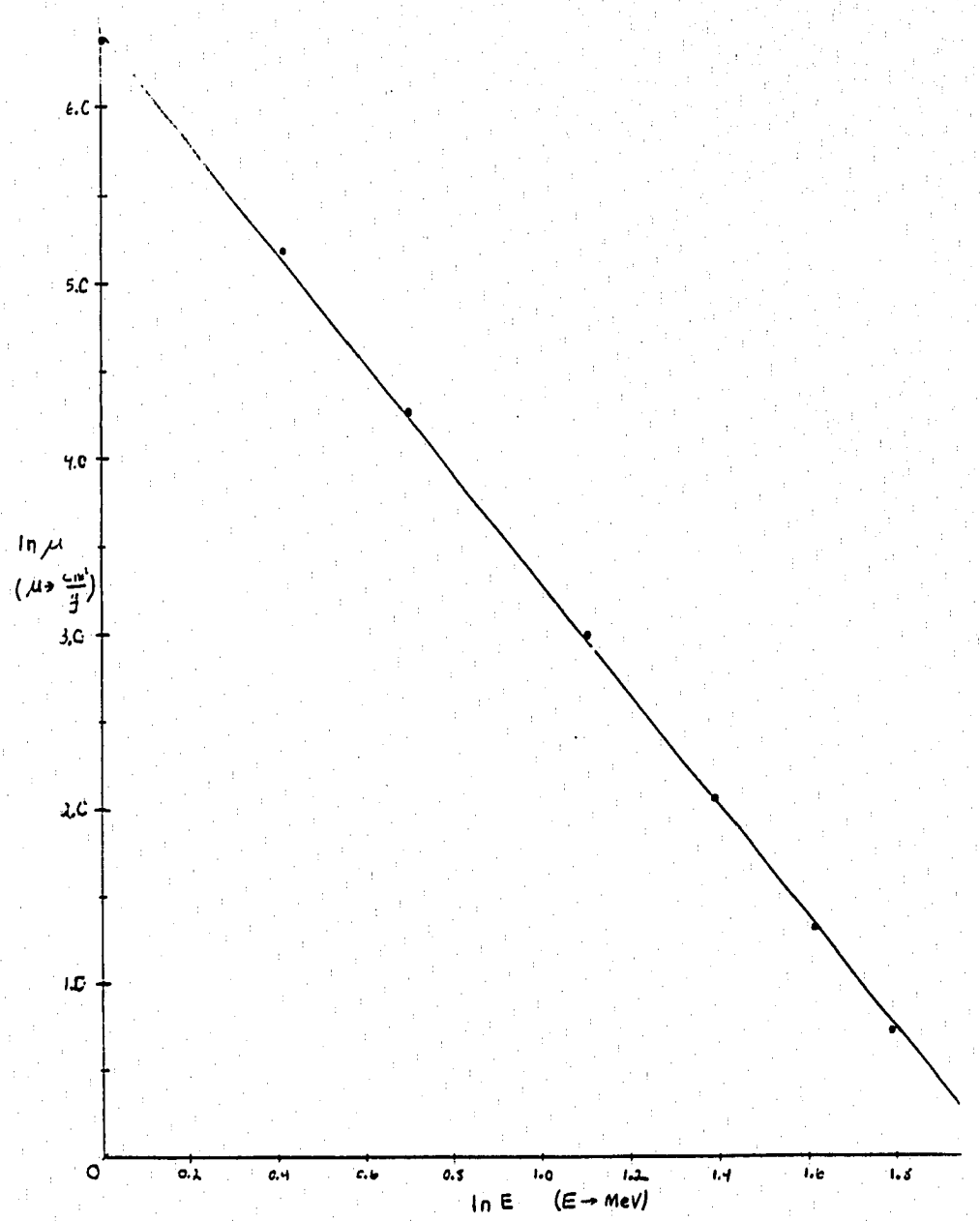

Figure 6. Plot of Mass Absorption Coefficient for ^{4}Be Window

APPENDIX D

Sample Calculation: 40 MeV S^{+13}+Ar Sulfur K_α X Ray

Equation (3B) in Appendix C gives an expression for calculating the cross section for the sulfur K_α x-ray.

$$\sigma_{S_{K_\alpha}} = 1.67 \times 10^{-12} \left(\frac{\Delta F}{\Delta P}\right)_{S_{K_\alpha}} \quad (cm^2)$$

It is now necessary to calculate the quantity $\left(\frac{\Delta F}{\Delta P}\right)_{S_{K_\alpha}}$:

$$\text{Let } \left(\frac{\Delta F}{\Delta P}\right)_{S_{K_\alpha}} \equiv \frac{\text{Change in the X-Ray Fraction, F}}{\text{Change in Gas Cell Pressure } (\mu)} \tag{1D}$$

$$S_{K_\alpha} \text{ x-ray Fraction, F} \equiv \frac{\text{Number of } S_{K_\alpha} \text{ X-Rays}}{\text{Number of Incident Ions, } I_0} \tag{2D}$$

The number of incident ions can be calculated by using the equation:

$$I_0 = \left(\frac{BCI}{100}\right) \left(\frac{\text{BCI Scale}}{e \cdot q_{ion}}\right) \cdot S \tag{3D}$$

The quantity of "BCI Scale" is the scale used in the BCI current integrator during these measurements.

Here BCI Scale = 2μA

The variables q_{ion} and e represent the total electric charge of each ion.

Here q_{ion} = +13 $\qquad$ e = 1.6021×10^{-19} coulombs

The quantity S represents a correction factor for small beam currents. When the signal input to the BCI current integrator was too small to register on the BCI, a Keithley multimeter was used in series with a 3 MΩ resistor to enable the BCI to record these small current readings.

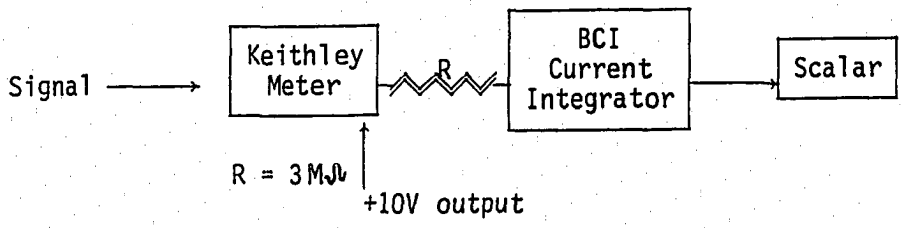

Maximum current through R = 3MΩ resistor:

$I_m = \frac{V}{R}$ V = +10 Volt Output, R = 3MΩ

$$I_m = \frac{10V}{3 \times 10^6 \Omega} = 3.33 \times 10^{-6} A$$

$$S = \frac{\text{Keithley Scale}}{I_m} = 3 \times 10^5 \text{ (Keithley Scale)}$$

Here Keithley Scale = $1 \times 10^{-10} A$

$$S = 3 \times 10^5 \cdot (1 \times 10^{-10})$$

$$\boxed{S = 3 \times 10^{-5}}$$

The additional factor of 100 in the denominator of equation (3D) represents a design parameter unique to the BCI itself. All of the constants listed above can now be combined together:

$$\boxed{I_0 = 2.881 \times 10^5 \text{ BCI}}$$

Sample Data:

Run	I_0 (x 10^9)	Counts S_{K_α} X Rays	F_{SULFUR} (x 10^{-7})	Pressure (μ)
14	3.455 ± 0.032	3064 ± 55	8.868 ± 0.167	46.9
15	4.583 ± 0.036	2469 ± 50	5.387 ± 0.117	29.7
16	5.330 ± 0.039	1445 ± 38	2.711 ± 0.074	15.2
17	6.726 ± 0.044	1242 ± 35	1.847 ± 0.053	10.0
18	8.486 ± 0.049	1018 ± 32	1.199 ± 0.038	7.1
19	15.252 ± 0.066	1025 ± 32	0.672 ± 0.021	3.4
20	2.458 ± 0.027	57 ± 8	0.232 ± 0.033	0

A plot of F_{SULFUR} versus Pressure can be found in Figure 7 on page 36. The quantity I_0 was calculated using BCI values. The variable F_{SULFUR} found in column four can be calculated using equation (2D). When this quantity is plotted against the gas cell pressure, the slope of the resulting line is $(\frac{\Delta F}{\Delta P})_{S_{K_\alpha}}$ in equation (1D). A least squares fitting program was used to calculate the value of each slope.

Here $(\frac{\Delta F}{\Delta P})_{S_{K_\alpha}} = 1.86 \pm 0.19 \times 10^{-8}\ \mu^{-1}$

The sulfur K_α x-ray cross section can now be calculated using equation (3B) in Appendix B.

$$\sigma_{S_{K_\alpha}} = 1.67 \times 10^{-12}\ \mu\cdot cm^2 (1.86 \pm 0.19) \times 10^{-8}\ \mu^{-1}$$

$$\therefore \boxed{\sigma_{S_{K_\alpha}} = (3.11 \pm 0.43) \times 10^{-20} cm^2}$$

The x-ray cross section can be calculated at the four measured energies using the procedure outlined above.

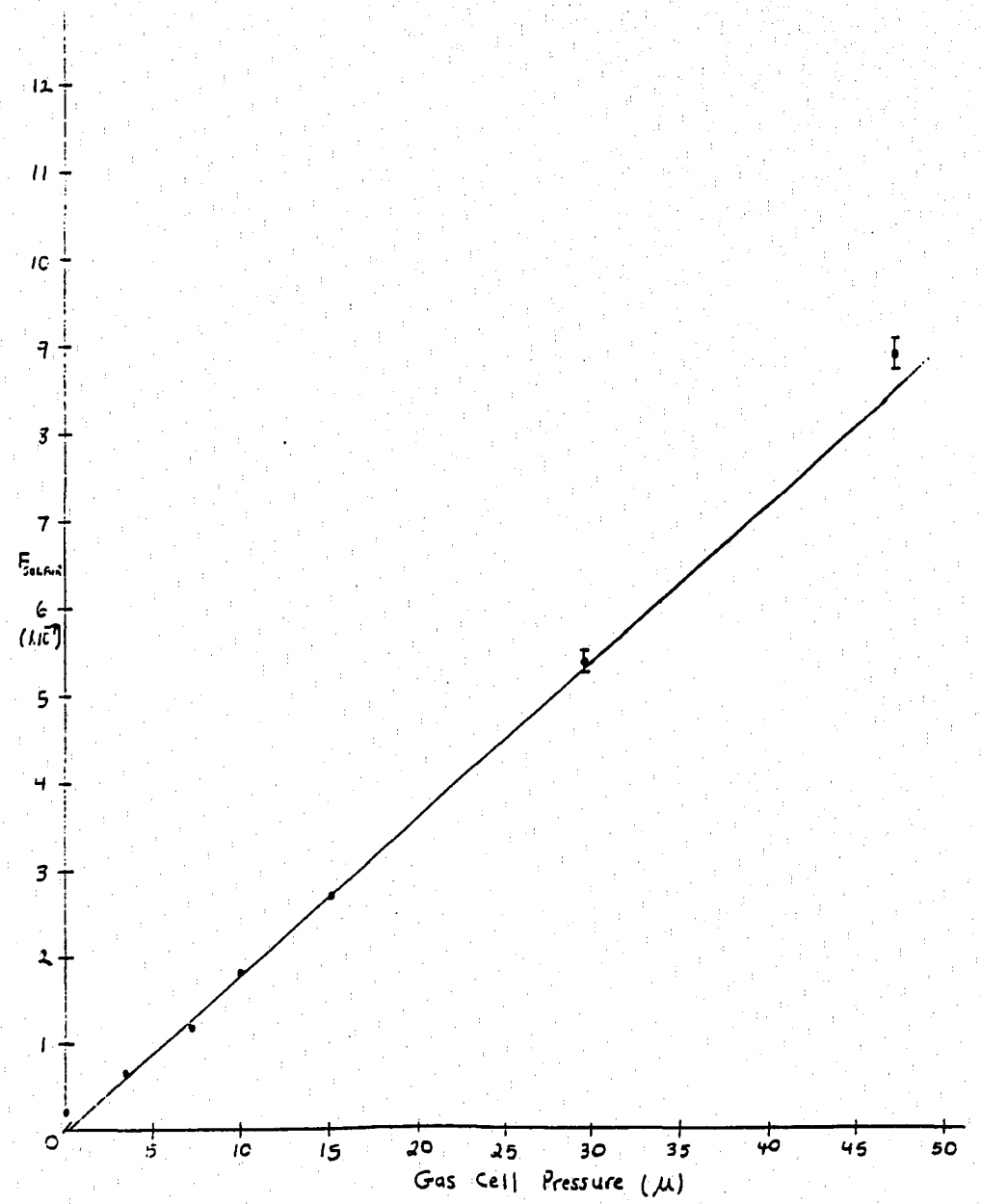

Figure 7. Plot of F_{SULFUR} Versus Gas Cell Pressure

BIBLIOGRAPHY

Acosta, V., Cowan, C.L., and Graham, B.J., Essentials of Modern Physics. New York: Harper and Row, Publishers, 1973.

Brandt, D., Phys. Rev. A 27, 1314 (1983).

Fano, U., and Fano, L., Basic Physics of Atoms and Molecules. New York: John Wiley and Sons, Inc., 1959.

Gerald, C.F., Applied Numerical Analysis. Reading: Addison-Wesley Publishing Co., 1978.

Loeb, L.B., Atomic Structure. New York: John Wiley and Sons, Inc., 1938.

Macdonald, J.R., Brown, M.D., Czuchlewski, S.J., Winters, L.M., Laubert, R., Sellin, I.A., and Mowat, J.R., Phys. Rev. A 14, 1997 (1976).

Storm, E., and Israel, H.I., Nuclear Data Tables, A 7, 565 (1970).

Tanis, J.A., Shafroth, S.M., Willis, J.E., Clark, M., Swenson, J., Strait, E.N., and Mowat, J.R., Phys. Rev. Lett. 47, 828 (1981).

Tanis, J.A., Bernstein, E.M., Graham, W.G., Clark, M., Shafroth, S.M., Johnson, B.M., Jones, K.W., and Meron, M., Phys. Rev. Lett. 49, 1325 (1982).

Veldre, V.Y., ed., Atomic Collisions, The Theory of Electron-Atom Collisions. Cambridge: The M.I.T. Press, 1963.

Weast, R.C., and Astle, M.J., eds., CRC Handbook of Chemistry and Physics, 59th Edition. Palm Beach: CRC Press, Inc., 1979.

Winters, L., Brown, M.D., Ellsworth, L.D., Chiao, T., Pettus, E.W., and Macdonald, J.R., Phys. Rev. A 11, 174 (1975).